IEEE Access
Multidisciplinary | Rapid Review | Open Access Journal

Received May 16, 2019, accepted June 3, 2019, date of publication June 26, 2019, date of current version July 17, 2019.

Digital Object Identifier 10.1109/ACCESS.2019.2924994

Improved Mode-Adaptive Droop Control Strategy for the DC Microgrid

JAFAR MOHAMMADI, (Student Member, IEEE), AND FIROUZ BADRKHANI AJAEI, (Member, IEEE)
Electrical and Computer Engineering Department, Western University, London, ON N6A 5B9, Canada

Corresponding author: Firouz Badrkhani Ajaei (fajaei@uwo.ca)

This work was supported by the Natural Sciences and Engineering Research Council of Canada under Discovery Grant RGPIN-2017-04772.

ABSTRACT The mode-adaptive droop control (MADC) strategy enables bus voltage regulation and power sharing between the distributed energy resources (DERs) in the direct current (dc) microgrid without communication systems. The conventional MADC strategy may fail to provide acceptable voltage regulation and power sharing performance in large dc microgrids where the voltage drops across the dc lines are not negligible. This paper proposes an improved MADC strategy for the dc microgrid. The proposed control strategy minimizes the adverse effects of the aforementioned voltage drops on the bus voltage regulation and the power sharing between the DERs in the dc microgrid. The performance of the proposed control strategy is investigated under various operating conditions and disturbance scenarios, using a detailed and realistic dc microgrid study system that is modeled in the PSCAD/EMTDC software environment. The study results indicate that the proposed control strategy: 1) effectively maintains the power balance in the dc microgrid; 2) accurately regulates the dc bus voltages under various operating conditions; 3) improves power sharing between the DERs without using communication systems; 4) significantly reduces the circulating currents between the DERs in the islanded microgrid; and 5) enhances the dc microgrid reliability, flexibility, modularity, and scalability.

INDEX TERMS DC microgrid, mode-adaptive droop control (MADC), power sharing, voltage regulation.

I. INTRODUCTION

The microgrid technology facilitates the grid integration of distributed energy resources (DERs) in power systems, reduces the energy loss, and provides reliable and high-quality electrical energy to consumers [1]–[3]. The direct current (DC) microgrid offers significant potential advantages over its alternating current (AC) counterpart. These advantages include (i) lower investment cost and power conversion losses due to elimination of unnecessary AC/DC converters, (ii) lower cable losses due to absence of skin effect, (iii) higher reliability and resilience to utility-side disturbances, and (iv) elimination of the need for frequency, phase, and reactive power controllers [4], [5]. The DC microgrid requires an effective control strategy to enable power sharing among its DERs, limit bus voltage deviations, maintain its stability, and provide an acceptable dynamic response to disturbances. The existing control strategies can be classified into the communication-based and non-communication-based categories [6]–[9].

The communication-based, i.e., centralized [10], [11], master-slave [12], circular chain [13], distributed [14]–[16], and hierarchical [17]–[19], control strategies provide desirable power sharing and voltage regulation performances. However, they require communication systems that are costly, vulnerable failure, and degrade system reliability, flexibility, modularity, and expandability [7]–[9], [20]. Therefore, the control strategies that rely on communication systems are more suitable for application in DC microgrids with fixed and compact configurations.

The control strategies in the non-communication based category enable power sharing among DERs using locally measured bus voltages. They offer advantages such as simple implementation, low cost, as well as high modularity, flexibility, expandability, and reliability [7]–[9], [20]. Therefore, the control strategies that do not rely on

The associate editor coordinating the review of this manuscript and approving it for publication was Reinaldo Tonkoski.

communication systems are more suitable for application in some of the emerging DC microgrids with multiple geographically dispersed DERs. The non-communication based category includes conventional droop control [20]–[22], improved droop control [23]–[26], DC bus signaling (DBS) [27]–[37], and mode-adaptive droop control (MADC) [38]–[43] strategies.

A conventional droop-controlled DER utilizes a fixed droop gain for the entire range of the DC-terminal voltage. Thus, the values of the droop gains significantly affect the microgrid stability, voltage regulation, and power sharing accuracy. A small gain results in more accurate voltage regulation and less accurate power sharing among the DERs, and vice versa [20]–[22]. To resolve these issues, a variety of improved droop control strategies have been proposed. The nonlinear droop controller of [23] improves the power sharing performance but adds complexity and nonlinearity to the control system. The adaptive droop control strategy of [24]–[26] reduces the circulating currents and the power sharing mismatch among the DERs. However, it is sensitive to the line parameters and also becomes complex as the number of DERs increases.

The DBS and MADC strategies offer considerable performance improvement by using control characteristics that adapt to the microgrid operating conditions. Both of these decentralized control strategies operate using locally measured bus voltages.

The DBS control strategy [27]–[37] utilizes multiple predefined DC voltage ranges to determine the operation modes of the DERs and the grid-tied converter (GTC). The operation mode of each component changes instantaneously whenever the corresponding bus voltage enters any of the aforementioned ranges. In [44], a detailed review of the existing DBS control strategies is provided and a versatile DBS control strategy is introduced. The main shortcoming of the DBS control strategy is the fact that it utilizes non-overlapping operating voltage ranges to achieve coordinated control of the renewable energy sources (RESs), the battery energy storage systems (BESSs), and the GTC. This may cause unnecessary curtailment of the renewable energy generation and reduced energy storage by the BESSs, under specific operating conditions, as demonstrated in Section IV of this paper.

The MADC strategy utilizes a hysteresis characteristic to switch between voltage control by the RESs and the BESSs in the islanded microgrid, depending on the bus voltage variations [38]–[43]. The conventional MADC strategy is designed based on the assumption that all DERs measure equal bus voltages, neglecting the voltage drops caused by the line resistances. This is not always a valid assumption. Thus, the conventional MADC strategy may fail to provide acceptable coordination between the voltage controlling components in the islanded DC microgrid, as demonstrated and discussed in Section IV. This issue degrades the power sharing and voltage regulation in the DC microgrid.

This paper proposes an improved MADC strategy that minimizes the adverse effects of unequal bus voltages on the coordinated participation of the DERs in regulating bus voltages and maintaining the power balance in the DC microgrid. The proposed control strategy does not require communication systems. The performance of the proposed MADC strategy is comprehensively investigated using a detailed and realistic DC microgrid study system. The study system includes multiple DERs that are dispersed across non-ideal feeders, i.e., feeders with considerable resistances. The study results highlight the shortcomings of the conventional MADC strategy and also indicate that the proposed improved MADC strategy:

- effectively maintains the power balance in the microgrid under large disturbances.
- accurately regulates the DC bus voltages under various operating conditions.
- improves power sharing among the DERs.
- improves the DC microgrid stability and dynamic response to disturbances.
- enhances the DC microgrid reliability, flexibility, modularity, and scalability.

II. CONVENTIONAL MADC STRATEGY

In the conventional MADC strategy, the GTC regulates the bus voltages of the grid-connected DC microgrid. The bus voltage regulation in the islanded DC microgrid is performed by the DERs, i.e., the RESs and the BESSs, since the GTC is unable to exchange power with the AC grid. Thus, each DER in the islanded DC microgrid operates in one of the following two modes [38], [39].

- *Mode I:* In this operation mode, the BESSs regulate the DC bus voltages using their droop characteristics, while the RESs utilize their MPPT controllers to maximize the harvested energy.
- *Mode II:* This mode is activated when the BESSs are unable to prevent excessive over-voltages by absorbing their maximum powers. Hence, the power balance is maintained and the bus voltages are regulated by curtailing the power outputs of the RESs using droop characteristics.

The operation mode of each DER is determined depending on its DC bus voltage, using the hysteresis characteristic of Fig. 1. When the voltage falls below the predefined threshold V_{th1}, the operation mode is switched to *Mode I*, and when the voltage exceeds the threshold V_{th2}, the DER operation mode is switched to *Mode II* [38], [39]. In an ideal DC microgrid, the DC voltages seen by all DERs are almost equal. In such a system, depending on the MADC mode, either all BESSs or all RESs participate in regulating the bus voltages.

In a practical DC microgrid, where the voltage drops across the feeders may cause the bus voltages to be considerably different, some of the DERs may fail to switch to the appropriate operation mode when it is necessary. This takes place when

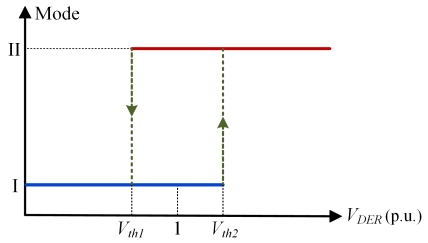

FIGURE 1. Mode switching characteristics of the conventional MADC strategy.

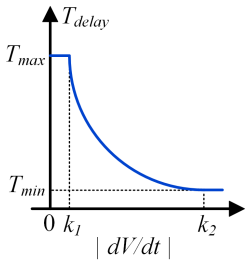

FIGURE 2. Variations of the adaptive time delay with respect to ROCOV.

a relatively large DER switches to the voltage regulation mode, i.e., *Mode I* for the BESSs and *Mode II* for the RESs, before the other DERs do so. The resulting improvement in the voltage profile of the microgrid may prevent some other DERs from performing the appropriate mode change, as shown in Section IV. This issue may lead to unacceptable power sharing performance and poor dynamic response to disturbances.

III. IMPROVED MADC STRATEGY

In this section, an improved MADC strategy is proposed to address the mode switching issues of the conventional MADC strategy. The aforementioned improvement is made using an adaptive mode switching algorithm and appropriate DER control systems.

A. ADAPTIVE MODE SWITCHING ALGORITHM

The main idea is to delay all mode change actions such that none of the BESSs (RESs) attempts to change its operation mode in response to a voltage disturbance, before all other BESSs (RESs) detect the disturbance. The delay must be sufficiently large to ensure that all bus voltages will reach the mode change threshold, before the first DER changes its operation mode. The delay must also be sufficiently small to ensure that all of the bus voltages remain within the acceptable range. Thus, the adaptive time delay of (1), which depends on the rate of change of voltage (ROCOV), is utilized to satisfy the aforementioned constraints.

$$T_{delay} = \begin{cases} T_{max}, & if\ 0 < \left|\dfrac{dV_{dc}}{dt}\right| < k_1 \\ \dfrac{\Delta V}{|dV/dt|}, & if\ k_1 \le \left|\dfrac{dV_{dc}}{dt}\right| \le k_2 \\ T_{min}, & if\ k_2 < \left|\dfrac{dV_{dc}}{dt}\right| < \infty \end{cases} \quad (1)$$

The parameter $\Delta V = min\ ((V_{max} - V_{th2}), (V_{th1} - V_{min}))$ represents the voltage change caused by the delayed mode switching, before the voltage reaches its upper limit V_{max} or lower limit V_{min}. The maximum and minimum values of the adaptive time delay T_{delay} are denoted by T_{max} and T_{min}, respectively. The constants $k_1 = \Delta V/T_{max}$ and $k_2 = \Delta V/T_{min}$ are the values of the ROCOV at which the T_{delay} reaches the aforementioned maximum and minimum values, respectively. Under large disturbances, where the ROCOV is significant, the T_{delay} becomes shorter and allows faster mode switching to limit the voltage deviation. Under small disturbances, where the ROCOV is insignificant, the T_{delay} becomes longer and enables mode switching of all DERs. Fig. 2 shows the variations of the adaptive time delay T_{delay} with respect to the ROCOV. Fig. 3 shows the mode switching characteristics of the improved MADC strategy.

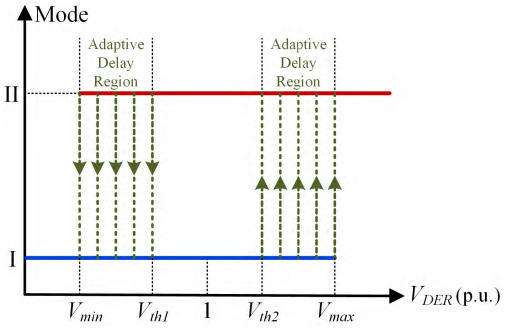

FIGURE 3. Mode switching characteristics of the improved MADC.

The parameters of the proposed MADC strategy, i.e., V_{min}, V_{max}, V_{th1}, V_{th2}, T_{min}, and T_{max} should be selected carefully. The values of the upper and lower voltage limits V_{max} and V_{min} are assumed to be 1.1 p.u. and 0.9 p.u., respectively. Adopting a much larger V_{max} or a much smaller V_{min} may cause power quality issues (excessive over-voltage or under-voltage conditions). The voltage thresholds V_{th1} and V_{th2} affect the adaptive mode changing performance. Choosing voltage thresholds that are too close to the aforementioned voltage limits leads to a small voltage margin ΔV in (1), and disables the adaptive adjustment of the mode changing time delay. On the other hand, using voltage thresholds that are too close to 1 p.u. should be avoided, since sensor inaccuracy and voltage ripples could cause oscillatory behavior [38], [39]. Under normal operating conditions, the bus voltage deviations caused by voltage drop across the lines can be as high as ±0.05 per-unit. Thus, choosing voltage thresholds in the ranges of $V_{min} \le V_{th1} \le 0.95$ p.u. and 1.05 p.u. $\le V_{th2} \le V_{max}$ is recommended. In microgrids with short lines, where the line voltage drops are lower than 0.05 p.u., values closer to 1 p.u. can be chosen for the voltage thresholds. The time delays T_{min}, and T_{max} are determined such that reliable mode changing performance is achieved without causing excessively long delays in voltage regulation.

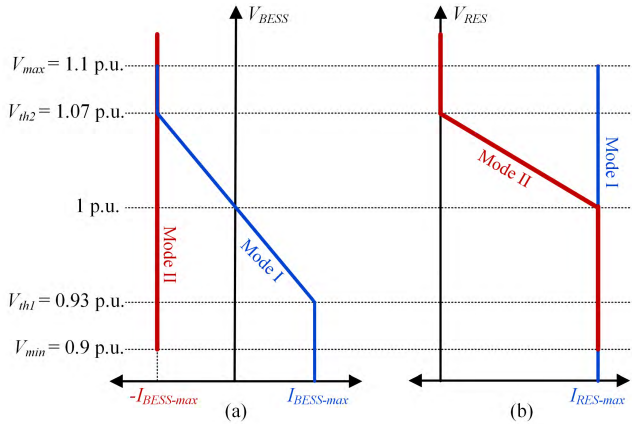

FIGURE 4. *V-I* characteristics of the DERs, (a) BESS, and (b) RES.

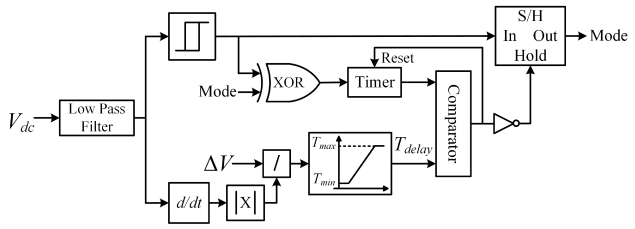

FIGURE 5. Block diagram of the adaptive mode switching algorithm.

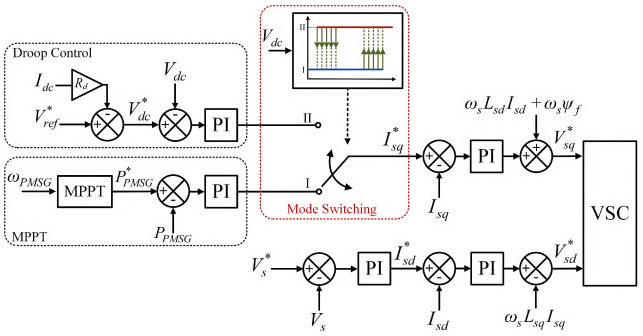

FIGURE 6. Control block diagram of the PMSG-type WT.

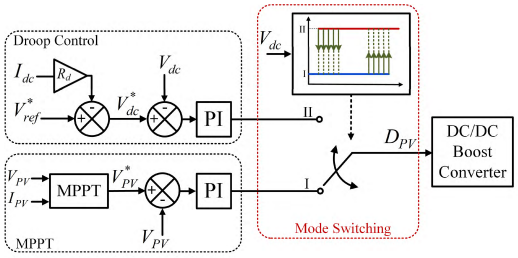

FIGURE 7. Control block diagram of the PV generation system.

Fig. 4 shows the *v-i* characteristics of the DERs in both operation modes. This figure illustrates that all DERs (RESs and BESSs) utilize two modes of operation. In Mode I, all RESs operate in the MPPT mode and all BESSs operate within their current limits to regulate their DC bus voltages. In Mode II, all BESSs operate in the charging mode and all RESs operate within their current limits to regulate their DC bus voltages.

The block diagram of the proposed adaptive mode switching algorithm is shown in Fig. 5. The hysteresis block in Fig. 5 represents the conventional mode switching algorithm and generates a mode signal that can be either I or II. The timer is enabled to count whenever the output of the hysteresis block is not the same as the current operation mode. The comparator output becomes high as soon as the timer output exceeds the adaptive delay of (1), and thereby allows the Sample-and-Hold (S/H) block to refresh its output and perform the mode switching. As shown in Fig. 5, a fourth-order Butterworth low-pass filter with the cut-off frequency of 500 Hz is applied to the voltage signal to reduce the adverse effects of noise and switching ripples.

B. DER CONTROL SYSTEMS

This sub-section introduces the DER control systems utilized by the proposed improved MADC strategy.

1) WT CONTROL

The control system of the permanent magnet synchronous generator (PMSG)-type wind turbine (WT) considered in this paper includes a pitch angle controller and the voltage source converter (VSC) controller. The former limits the aerodynamic torque and keeps the turbine speed in a limited range. The latter is based on the vector control method in the *dq* reference frame. Depending on the MADC mode, the VSC controls the PMSG active power to achieve MPPT or to regulate the DC voltage. The VSC also controls the reactive power to regulate the stator terminal voltage [41], [44]. The WT control system is shown in Fig. 6, where V^*_{ref} and R_d are the DC bus voltage reference and the droop gain, respectively.

2) PV CONTROL

Each photovoltaic (PV) generation unit either generates its maximum power using an MPPT controller or regulates the DC bus voltage, depending on the MADC mode. A general perturbation and observation MPPT method is implemented for the PV system [41], [44]. The control block diagram of the PV system is shown in Fig. 7.

3) BESS CONTROL

Each BESS either operates in the charging mode or participates in regulating the DC bus voltage, depending on the MADC mode. A BESS must operate within a range of voltage and state-of-charge (SOC) set-values to protect and maximize the lifetime of its elements [41], [44]. The control block diagram of each BESS is shown in Fig. 8.

The stability of the DC microgrid and its dynamic response to disturbances depend on the parameters of the proportional-integral (PI) controllers shown in Figs. 7-8. These controllers can be optimally tuned using model-based methods [45] as well as meta-heuristic algorithms [46], [47].

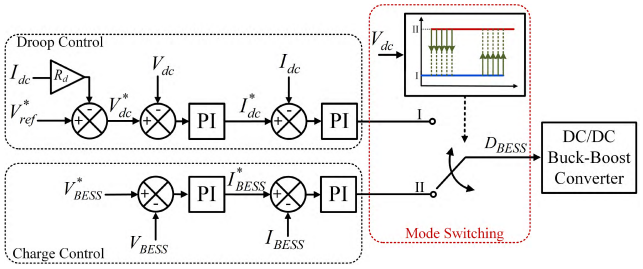

FIGURE 8. Control block diagram of the BESS.

As shown in Figs. 6-8, the control mode change is performed by switching between the outputs of different PI controllers. The mode switching action may cause a sudden change in the controller output signal, if the outputs of the two PI controllers are not equal at the switching time instant. Smooth mode switching can be achieved by automatically setting the initial conditions of the inactive PI controller (the one that becomes active after mode switching) in accordance with the output value of the active controller, at the moment of controller switching [43].

IV. STUDY RESULTS

This section investigates and compares the performance of the proposed improved MADC strategy with those of the conventional MADC strategy and the DBS control strategy. Comprehensive time-domain simulation studies are conducted in the PSCAD software using a detailed model of a realistic DC microgrid study system. The study system of Fig. 9, [44], is developed by converting the IEEE 37-node AC test system [48] to DC and enabling it to operate as a microgrid. The operating DC voltage is chosen to be ±750 V to comply with the guidelines of the IEC60038 standard for low-voltage DC systems [49].

The ±750 V DC microgrid includes a 1 MW PMSG-type WT connected to node 709, two 0.5 MW PV generation systems connected to nodes 712 and 722, and two 0.4 MW BESSs connected to nodes 705 and 707. A 2 MW GTC interfaces the DC microgrid with the AC grid through a 0.75kV/4.8kV transformer at node 701. All converters are represented in detail using switching models. The parameters of the study system, and the coefficients of the PI controllers of the DERs are provided in the Appendix.

In the following sub-sections, the performances of the conventional and improved MADC strategies are investigated and compared with each other under various disturbances that cause different levels of power imbalance in the DC microgrid study system of Fig. 9. The DER terminal (DC bus) voltages and output powers are reported in per-unit, to enable comparison and easier analysis of the study results. The base values for the DER powers and the bus voltages are the corresponding power ratings and the rated line-to-ground voltage of 750 V, respectively.

The parameters of the improved MADC strategy are $V_{th1} = 0.93$ p.u., $V_{th2} = 1.07$ p.u., $V_{min} = 0.9$ p.u., $V_{max} = 1.1$ p.u., $\Delta V = 0.03$ p.u., $k_1 = 0.03$ p.u./s, $k_2 = 3$ p.u./s,

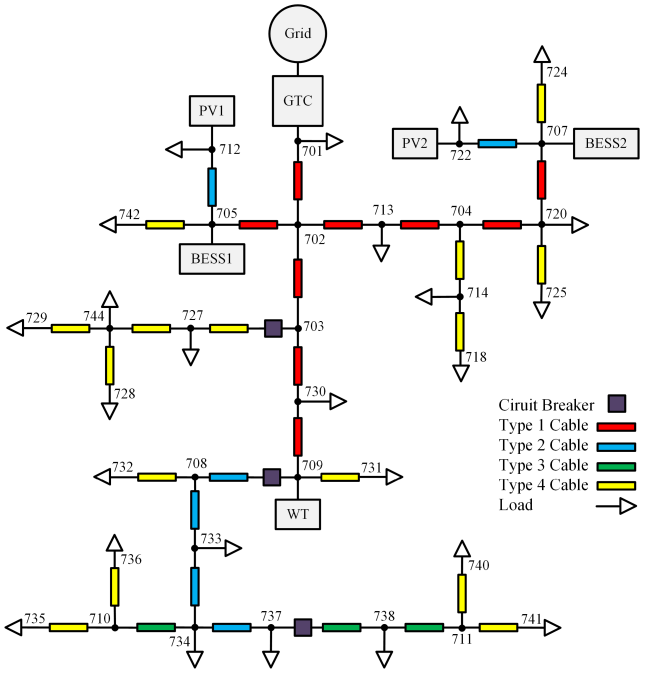

FIGURE 9. Single-line diagram of the study system.

$T_{min} = 0.01$ s, and $T_{max} = 1$ s. These values are determined based on the results of comprehensive simulation studies, to achieve the best performance.

A. CASE STUDY 1

The first case study investigates an unscheduled islanding scenario that leads to a large power surplus in the microgrid. Figs. 10 and 11 illustrate the performances of the conventional and improved MADC strategies, respectively. At $t < 0.5$ s, the microgrid is grid-connected, and the DER bus voltages are regulated by the GTC at values approximately between 1.02 p.u. and 1.05 p.u. All RESs operate in MPPT and generate 1 p.u. power, while the total power demand of the loads is 0.4 MW. Both BESSs operate in the charging mode and draw 1 p.u. power from the DC microgrid. As the total power generated by the RESs is larger than the total power demand in the DC microgrid, the GTC exports 0.75 MW to the AC grid.

At $t = 0.5$ s, the DC microgrid is islanded and the GTC power exchange with the AC grid becomes zero. Due to the resulting power surplus in the microgrid, all bus voltages start to rise at an almost equal rate. Therefore, all DERs are expected to switch to the *Mode II* described in Section II. This means, the BESSs must draw their maximum charging currents and the RESs must curtail their output powers in order to maintain the power balance in the microgrid and regulate the bus voltages.

As shown in Fig. 10, with the conventional MADC strategy, the WT changes its operation mode to *Mode II* as soon as its bus voltage reaches V_{th2} at $t = 0.508$ s. Consequently, the WT reduces its output power to 0.2 p.u. and

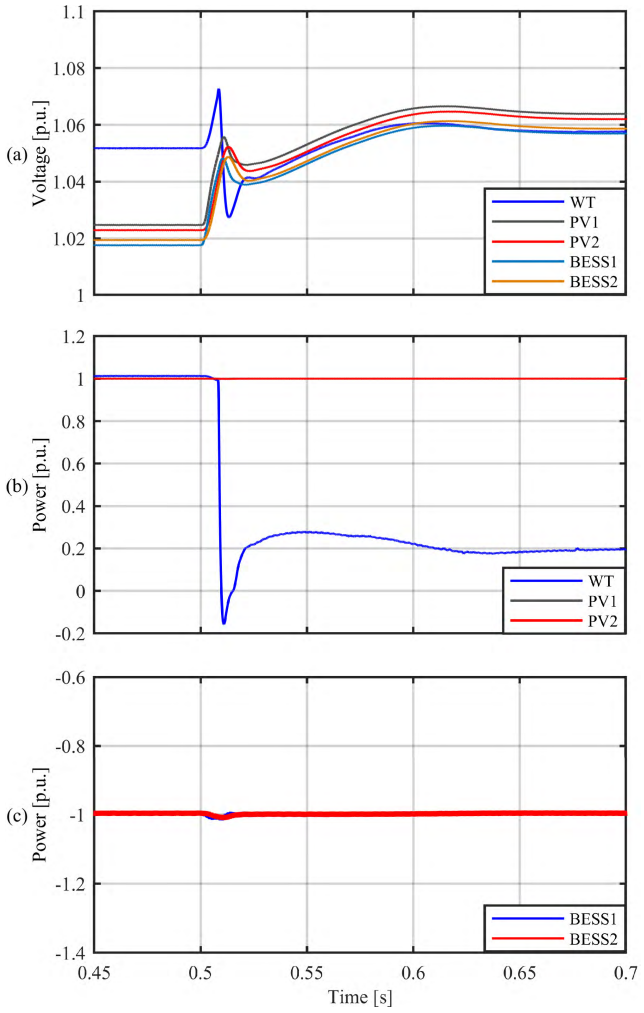

FIGURE 10. Performance of the conventional MADC strategy in *Case Study 1*: (a) DER bus voltages, (b) RES powers, (c) BESS powers.

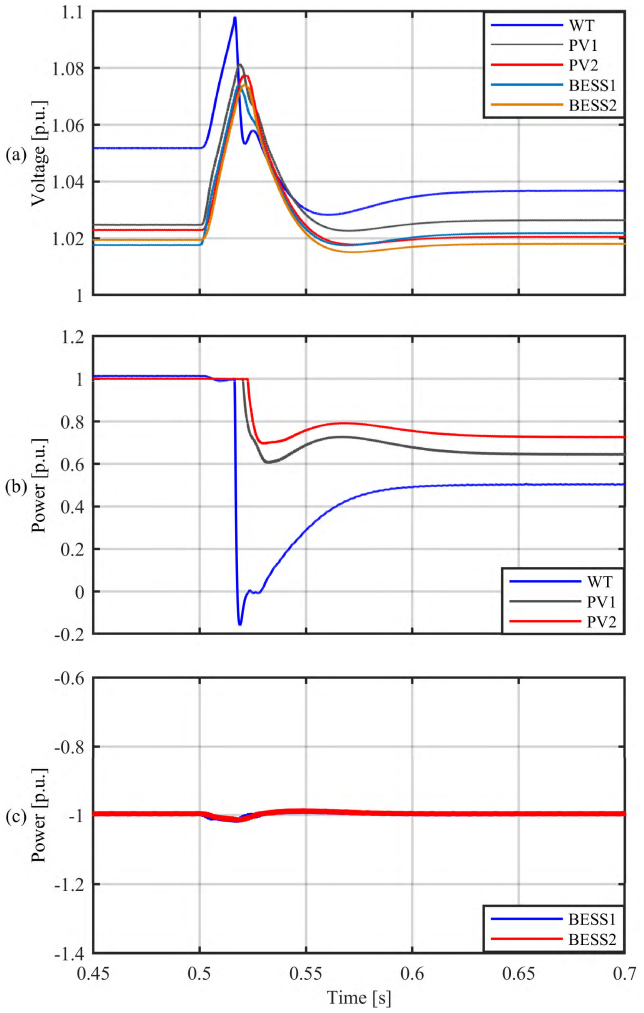

FIGURE 11. Performance of the improved MADC strategy in *Case Study 1*: (a) DER bus voltages, (b) RES powers, (c) BESS powers.

regulates the DER bus voltages at about 1.06 p.u. The two PV generation systems PV1 and PV2 fail to switch to the voltage control mode since their bus voltages do not reach the mode changing threshold V_{th2}. These results demonstrate that, when the conventional MADC strategy is implemented in a realistic DC microgrid, the faster reaction of a relatively large DER to a disturbance can desensitize some other DERs to that disturbance and prevent them from switching to the appropriate mode. This issue adversely affects the power sharing among the DERs, because the desensitized DERs, i.e., PV1 and PV2, do not participate in maintaining the power balance, as shown in Fig. 10 (b). This issue also leads to poor bus voltage regulation, as shown in Fig. 10(a) at $t > 0.6$ s, because the only voltage regulating component is the WT, i.e., PVs 1 and 2 do not participate in voltage regulation.

Fig. 11 shows that the proposed improved MADC strategy enables all RESs, i.e., the WT, the PV1, and the PV2, to switch to *Mode II* and participate in the voltage regulation. Consequently, all of the RESs reduce their output powers and regulate the DER bus voltages at values between 1.02 p.u. and 1.04 p.u. Fig. 11(b) shows that the proposed improved MADC does not achieve ideal power sharing, i.e., the output powers of the three RESs are not exactly equal. However, this issue is a limitation of non-communication-based control strategies, and is caused by unequal bus voltages in a realistic microgrid. Achieving ideal power sharing would require costly communication systems. Besides, the power sharing performance of the proposed MADC strategy is considerably better than that of the conventional MADC strategy.

Fig. 11(a) also shows that the proposed MADC strategy causes a slightly larger temporary voltage deviation before the mode switching takes place, i.e., at 0.51 s $< t <$ 0.52 s, as compared with the conventional MADC strategy of Fig. 10(a). This is due to the additional adaptive mode switching delay that is utilized to prevent the mode switching failure issue illustrated in Fig. 10(b). Allowing the bus voltages to continue to rise/fall for a short time period T_{delay} enables all DERs to detect the voltage variations and perform reliable mode switching. The utilized adaptive delay is determined by (1) such that the bus voltages do not reach the corresponding

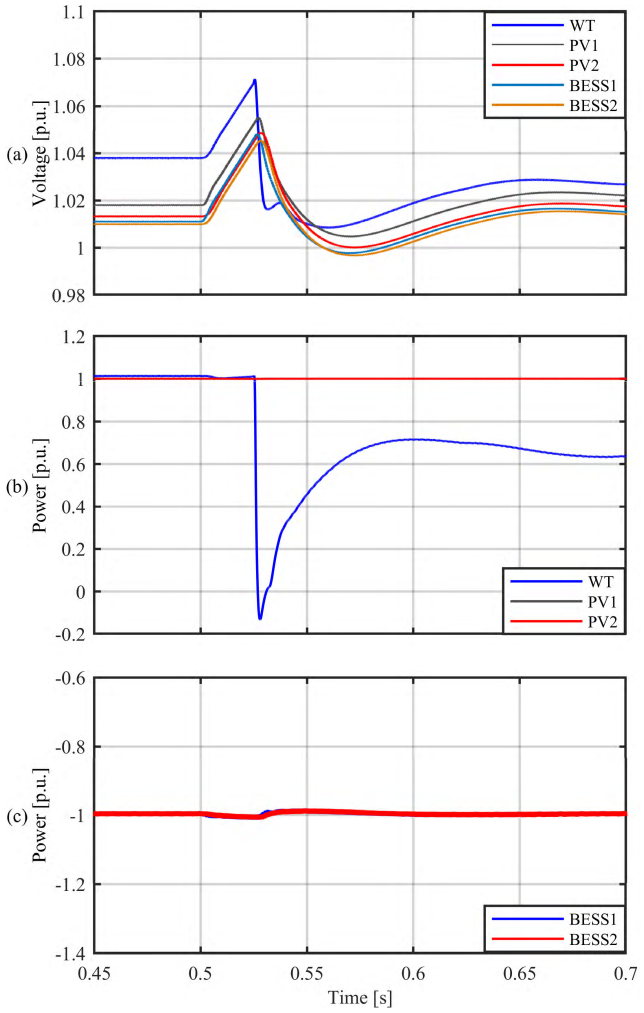

FIGURE 12. Performance of the conventional MADC strategy in *Case Study 2*: (a) DER bus voltages, (b) RES powers, (c) BESS powers.

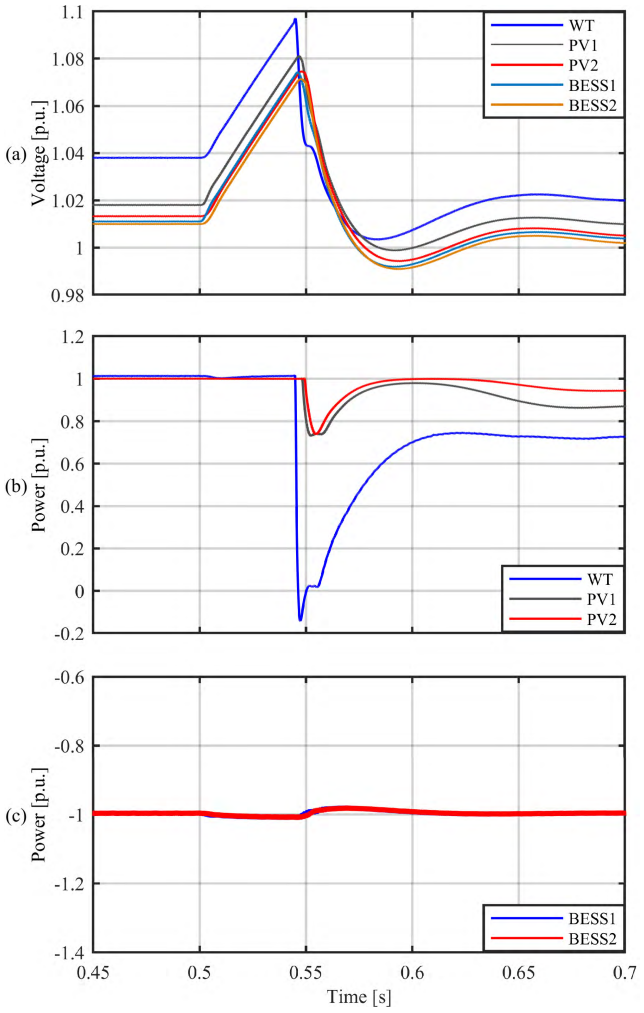

FIGURE 13. Performance of the improved MADC strategy in *Case Study 2*: (a) DER bus voltages, (b) RES powers, (c) BESS powers.

lower and upper limits which are assumed to be 0.9 p.u. and 1.1 p.u, respectively.

B. CASE STUDY 2

The second case study investigates the islanding scenario of Part *A*, but with different initial conditions. The main difference is that the total power demand of the loads in the grid-connected microgrid is increased to 0.85 MW. Hence, before islanding, the GTC exports 0.3 MW to the AC grid.

When the DC microgrid becomes islanded at $t = 0.5$ s, the power surplus in the microgrid is only 0.3 MW. The bus voltages rise at a rate that is lower than that of the *Case Study 1*. This case study mainly aims to demonstrate the necessity of utilizing a mode switching delay that is not fixed. Figs. 12 and 13 illustrate the performances of the conventional and improved MADC strategies, respectively.

As shown in Fig. 12, similar to the *Case Study 1*, the conventional MADC strategy fails to provide acceptable mode switching performance in this case. Only the WT changes its operation mode to voltage control, while the other RESs (the PV1 and the PV2) remain in *Mode I*, that is the MPPT mode. Due to the small power surplus, the WT is able to restore the power balance in the islanded DC microgrid and regulate all DER bus voltages at values between 1.01 p.u. and 1.03 p.u. However, the PV1 and the PV2 fail to participate in the voltage regulation, similar to the *Case Study 1*. This failure, which is illustrated in Figs. 10(b) and 12(b), forces the WT to curtail a larger portion of its output power.

Fig. 13 shows that, by utilizing a larger time delay due to the low ROCOV, the proposed improved MADC strategy enables all three RESs to detect the disturbance, switch to *Mode II*, and participate in the voltage regulation. Consequently, all RESs reduce their output powers and thereby regulate the DER bus voltages at values between 1.0 p.u. and 1.02 p.u. As expected, the BESSs continue to operate in the charging mode before and after the disturbance.

Fig. 13 shows that the performance of the improved MADC strategy is slightly better than that of the conventional MADC strategy, in terms of bus voltage regulation and power sharing among the RESs. This is due to the small

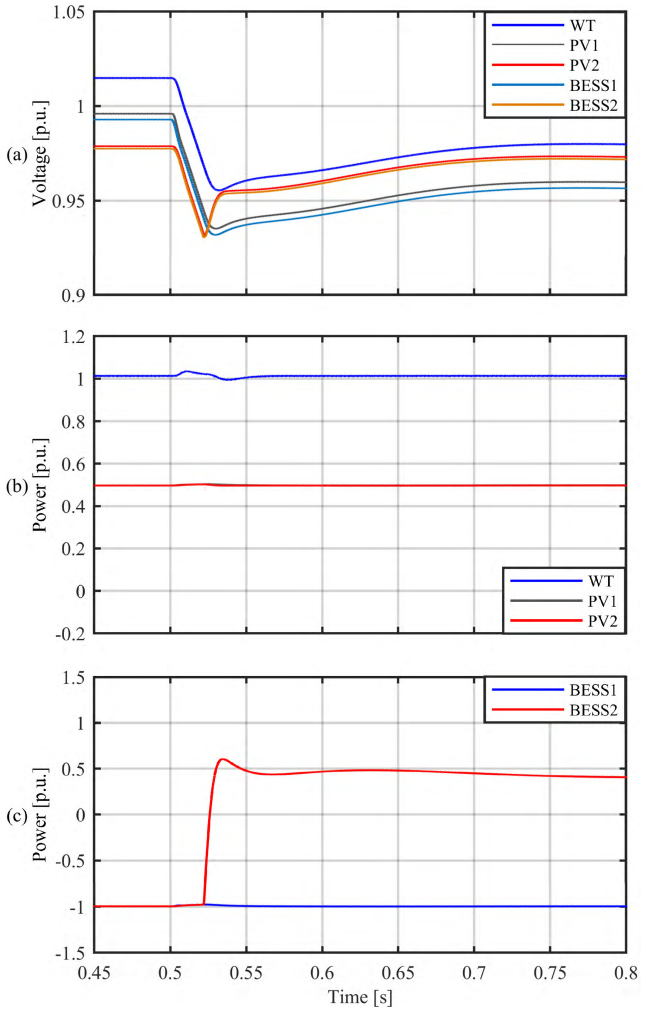

FIGURE 14. Performance of the conventional MADC strategy in *Case Study 3*: (a) DER bus voltages, (b) RES powers, (c) BESS powers.

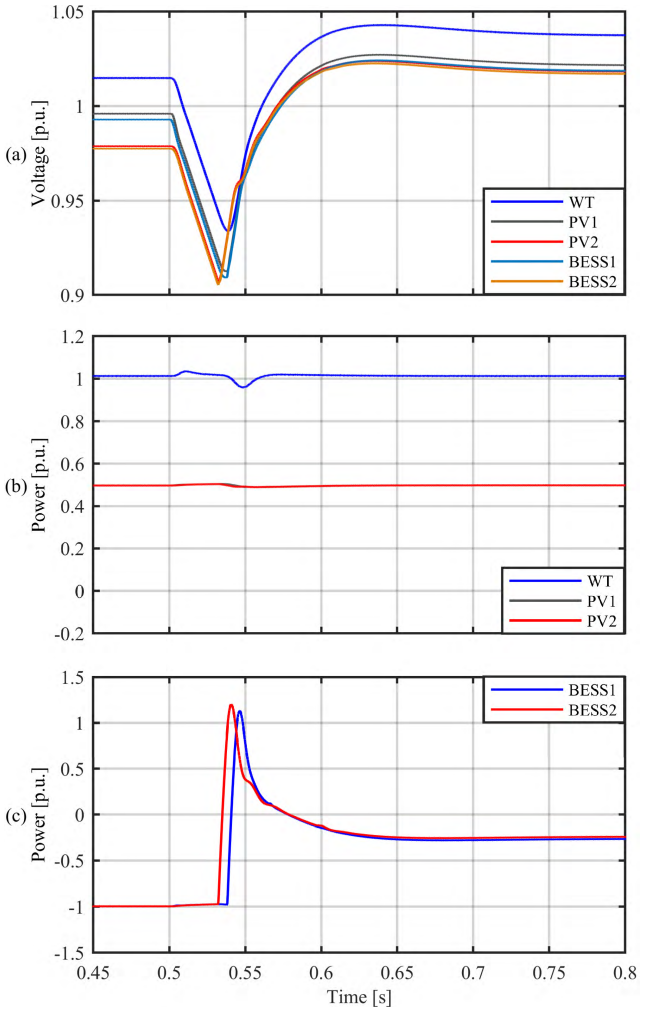

FIGURE 15. Performance of the improved MADC strategy in *Case Study 3*: (a) DER bus voltages, (b) RES powers, (c) BESS powers.

power imbalance of 0.3 MW in the DC microgrid, which does not cause significant voltage deviations or large power curtailment by the RESs. The performance improvement is more significant when the power imbalance caused by the disturbance is large, e.g., *Case Study 1*.

The Case studies 1 and 2 highlight two important points. First, the conventional MADC strategy may fail to coordinate the mode switching actions of the RESs under both low and high rates of voltage rise. Second, the adaptive delay utilized by the proposed improved MADC strategy enables reliable and coordinated mode switching by all RESs, regardless of how fast the bus voltages change.

C. CASE STUDY 3

The third case study investigates and compares the performances of the conventional and improved MADC strategies during an islanding scenario that leads to a power deficit in the DC microgrid. Before $t = 0.5$ s, the microgrid is grid-connected, and the DER bus voltages are between 0.97 p.u. and 1.02 p.u. The WT, PV1, and PV2 operate in MPPT and generate 1, 0.5, and 0.5 p.u. power, respectively, while the total power demand of the loads is 1.25 MW. Both BESSs operate in the charging mode and draw 1 p.u. power. As the total power demand in the grid-connected microgrid is larger than the power generated by the RESs, the GTC imports 0.6 MW from the AC grid.

At $t = 0.5$ s, the microgrid is islanded. Due to the resulting 0.6 MW power deficit in the microgrid, all bus voltages start to fall at an almost equal rate. In this case study, all DERs are expected to switch to *Mode I* after islanding. Thus, after the islanding, the RESs are expected to continue to operate in MPPT and the BESSs are expected to adjust their power outputs in order to maintain the power balance and regulate the bus voltages.

As shown in Fig. 14, with the conventional MADC strategy, only the BESS2 changes its operation mode to voltage control, due to its lower bus voltage. Thus, the DER bus voltages are regulated by the BESS2 at values between 0.96 p.u. and 0.98 p.u., while the BESS1 fails to perform the necessary mode switching and does not

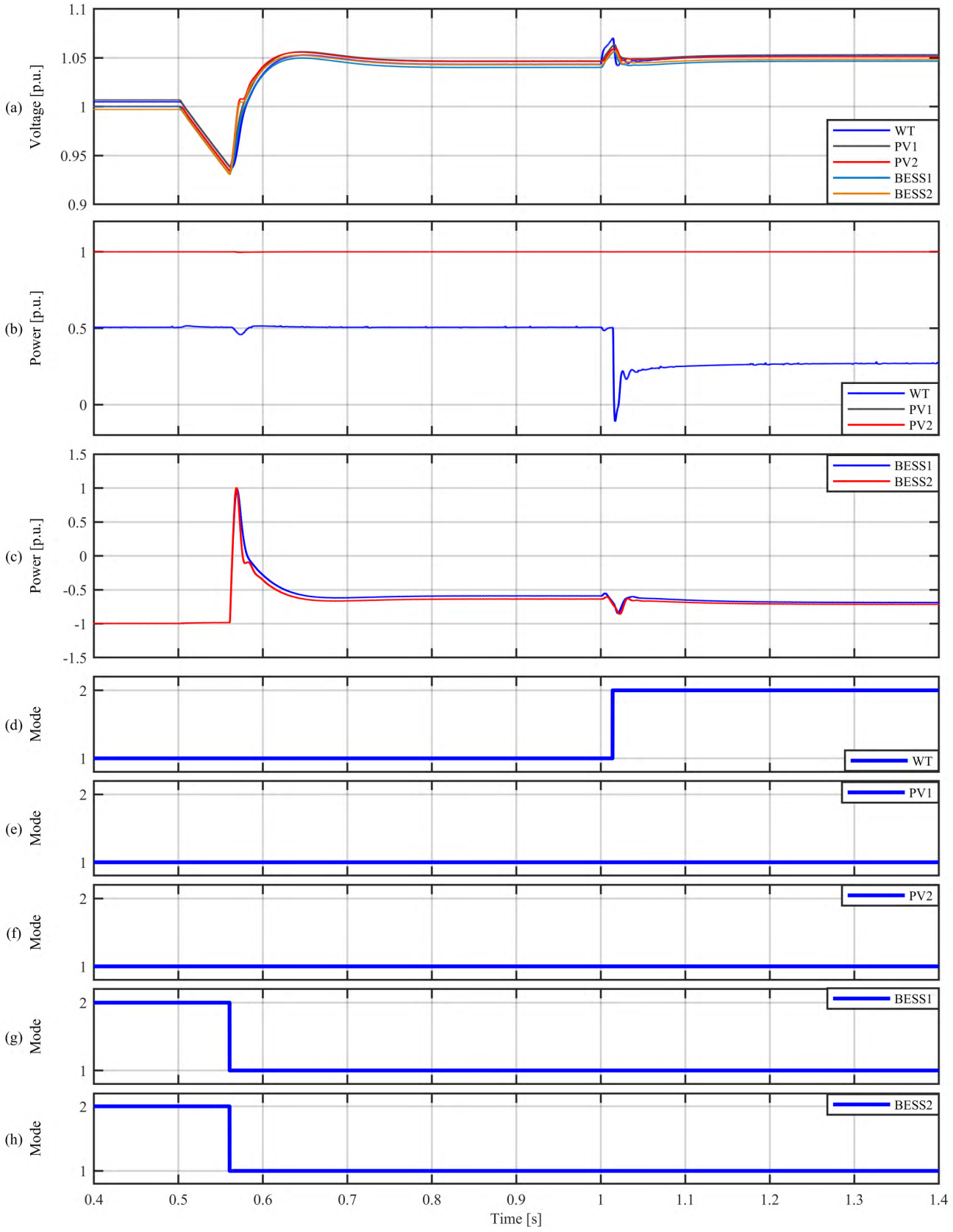

FIGURE 16. Performance of the conventional MADC strategy in *Case Study 4*: (a) DER bus voltages, (b) RES powers, (c) BESS powers, (d) WT operation mode, (e) PV1 operation mode, (f) PV2 operation mode, (g) BESS1 operation mode, (h) BESS2 operation mode.

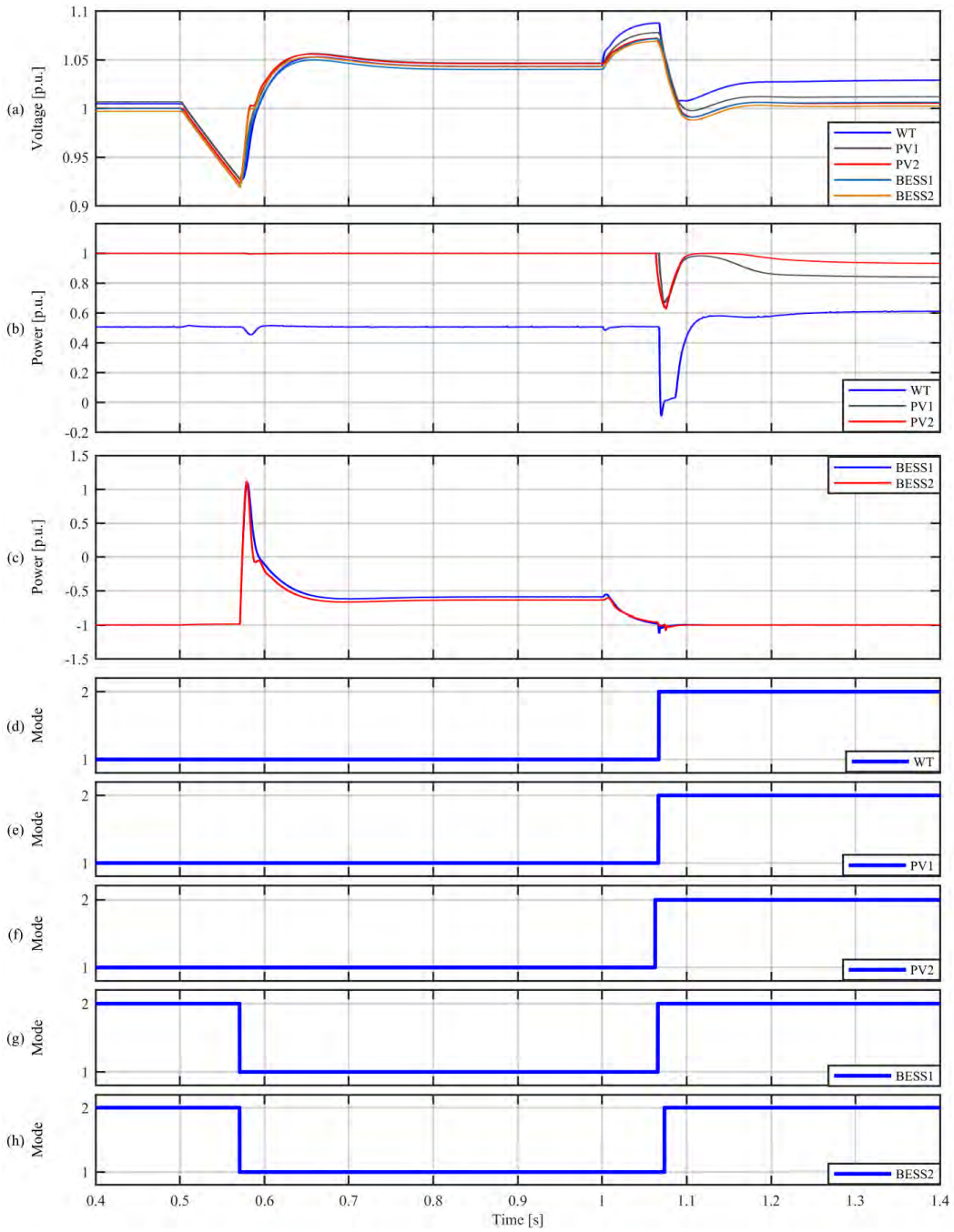

FIGURE 17. Performance of the improved MADC strategy in *Case Study 4*: (a) DER bus voltages, (b) RES powers, (c) BESS powers, (d) WT operation mode, (e) PV1 operation mode, (f) PV2 operation mode, (g) BESS1 operation mode, (h) BESS2 operation mode.

participate in the voltage regulation. In this case, the BESS1 is being charged in part by the BESS2, which increases the energy loss in the microgrid and causes faster discharge of the BESS2. The results of Fig. 14 indicate that the shortcomings of the conventional MADC strategy also apply to the mode switching performances of the BESSs.

Fig. 15 shows that the proposed improved MADC strategy enables both BESSs to participate in the voltage regulation and provide acceptable power sharing performance. Although the improvement in terms of reducing the voltage deviations is less significant in this specific case study, the fact that the BESSs perform desirable power sharing and do not cause circulating currents is a significant improvement.

D. CASE STUDY 4

The fourth case study investigates two successive disturbances with opposite effects in terms of the power balance in the microgrid. The first disturbance is an islanding scenario

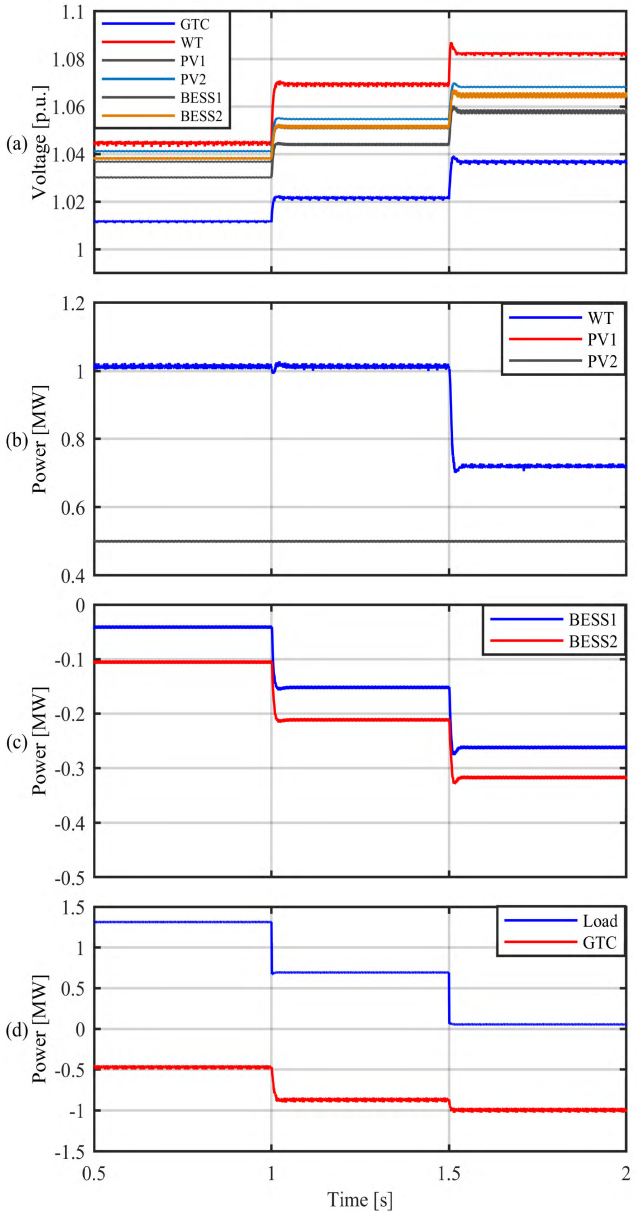

FIGURE 18. Performance of the DBS control strategy of [44] in *Case Study 5*: (a) DER bus voltages, (b) RES powers, (c) BESS powers, (d) GTC and load powers.

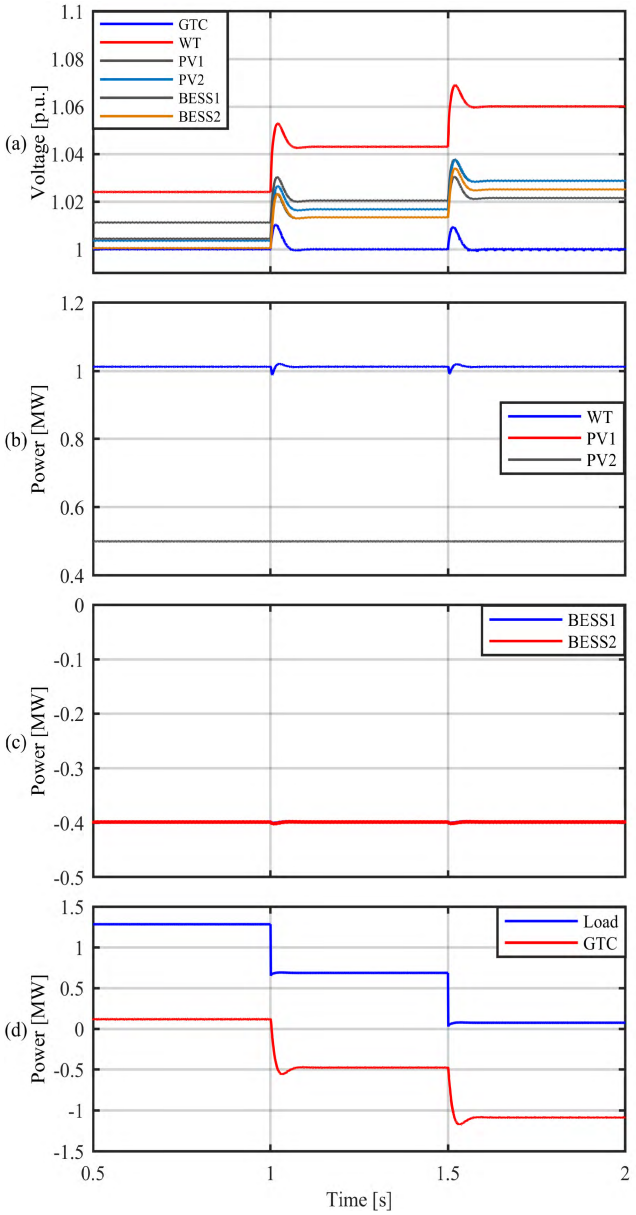

FIGURE 19. Performance of the improved MADC strategy in *Case Study 5*: (a) DER bus voltages, (b) RES powers, (c) BESS powers, (d) GTC and load powers.

that leads to a power deficit in the microgrid. The second disturbance is a load disconnection that causes a power surplus. Figs. 16 and 17 illustrate the performances of the conventional and improved MADC strategies, respectively. Before $t = 0.5$ s, the microgrid is grid-connected, and the DER bus voltages are regulated by the GTC at about 1 p.u. The WT, the PV1, and the PV2 operate in MPPT and generate 0.5, 1, and 1 p.u. power, respectively, while the total power demand of the loads is 0.97 MW. Both BESSs operate in the charging mode and draw 1 p.u. power from the microgrid. As the total power demand in the grid-connected microgrid is larger than the power generated by the RESs, the GTC imports 0.3 MW from the AC grid.

At $t = 0.5$ s, the microgrid is islanded and the GTC power exchange with the AC grid becomes zero. Due to the resulting power deficit in the microgrid, all bus voltages start to fall at an almost equal rate. Therefore, after the islanding, all of the DERs are expected to switch to *Mode I*. In other words, the RESs are expected to continue to operate in MPPT and the BESSs are expected to adjust their power outputs in order to maintain the power balance and regulate the bus voltages.

At $t = 1$ s, the circuit breaker at node 709 is tripped, which decreases the total power demand of the loads to 0.68 MW. Due to the resulting power surplus in the microgrid, all bus voltages start to rise. Therefore, all DERs are expected to switch to *Mode II* described in Section II. This means the

TABLE 1. Performances of the conventional and improved MADC strategies.

Case Study	MADC Strategy	Time (s)	DER Voltages (p.u.)	WT Power (p.u.)	PV1 Power (p.u.)	PV2 Power (p.u.)	BESS1 Power (p.u.)	BESS2 Power (p.u.)
1	Conventional	$t < 0.5$	1.02-1.05	1	1	1	-1	-1
		$t \geq 0.5$	1.06	0.2	1	1	-1	-1
	Improved	$t < 0.5$	1.02-1.05	1	1	1	-1	-1
		$t \geq 0.5$	1.02-1.04	0.5	0.64	0.72	-1	-1
2	Conventional	$t < 0.5$	1.01-1.04	1	1	1	-1	-1
		$t \geq 0.5$	1.01-1.03	0.65	1	1	-1	-1
	Improved	$t < 0.5$	1.01-1.04	1	1	1	-1	-1
		$t \geq 0.5$	1-1.02	0.74	0.87	0.94	-1	-1
3	Conventional	$t < 0.5$	0.97-1.02	1	1	1	-1	-1
		$t \geq 0.5$	0.96-0.98	1	1	1	-1	0.42
	Improved	$t < 0.5$	0.97-1.02	1	1	1	-1	-1
		$t \geq 0.5$	1.02-1.04	1	1	1	-0.27	-0.25
4	Conventional	$t < 0.5$	1	0.5	1	1	-1	-1
		$t \geq 0.5$	1.04-1.047	0.5	1	1	-0.6	-0.64
		$t \geq 1$	1.046-1.053	0.27	1	1	-0.7	-0.72
	Improved	$t < 0.5$	1	0.5	1	1	-1	-1
		$t \geq 0.5$	1.04-1.047	0.5	1	1	-0.6	-0.64
		$t \geq 1$	1-1.03	0.6	0.84	0.93	-1	-1

BESSs must draw their maximum charging currents and the RESs must curtail their output powers in order to maintain the power balance and regulate the bus voltages.

As shown in Fig. 16, after the islanding, the conventional MADC strategy enables both BESSs to change their operation modes to *Mode I*. The BESS1 and the BESS2 reduce their absorbed powers from 1 p.u. to 0.6 p.u. and 0.64 p.u., respectively, and regulate the DER bus voltages at values between 1.04 p.u. and 1.047 p.u. However, after the load disturbance (at $t > 1$ s), only the WT changes its operation mode to *Mode II*. The WT reduces its output power from 0.5 p.u. to 0.27 p.u. and regulates the DER bus voltages at values between 1.046 p.u. and 1.053 p.u. After the load disturbance, the PVs and the BESSs fail to switch to *Mode II*, because their bus voltages do not reach the mode changing threshold V_{th2}. This issue adversely affects the power sharing between the DERs, because the PVs do not participate in maintaining the power balance, as shown in Fig. 16 (b). The study results shown in Fig. 16 also indicate that the conventional MADC strategy leads to unnecessary curtailment of the renewable energy generated by the WT, since the batteries could absorb a larger amount of power (at $t > 1$ s).

Fig. 17 shows that, before the load disturbance is applied at $t = 1$ s, the proposed improved MADC strategy operates similar to the conventional MADC strategy (both satisfactory). However, after the load disturbance, the former provides a much more acceptable performance by enabling all DERs to switch their operation modes to *Mode II*. Using the proposed control strategy, in response to the power surplus at $t > 1$ s, both BESSs draw their maximum charging currents and all RESs participate in regulating the bus voltages by adjusting their output powers. The Case study 4 highlights the capability of the proposed control strategy in maintaining the power balance in the microgrid, facilitating power sharing among the DERs, and maximizing the generated renewable energy, under successive disturbances that may have opposite effects.

Table 1 compares the mode switching performances of the conventional and improved MADC strategies under the *Case Studies 1-4*.

E. CASE STUDY 5

The fifth case study investigates and compares the performances of the proposed MADC strategy and the DBS control strategy of [44] under the same load disturbance, i.e., *Case Study 1* of [44]. The total power demand by the loads is reduced and the grid-connected DC microgrid has to handle the resulting large power surplus.

As shown in Fig. 18, with the DBS control strategy, before $t = 1$ s, the grid-connected DC microgrid is in steady-state, and the DER terminal voltages are between 1.01 and 1.045 p.u. The WT, PV1 and PV2 operate in MPPT mode and generate 1, 0.5 and 0.5 MW power, respectively, while the total power demand is 1.31 MW. The BESS1 and BESS2 draw 0.04 and 0.1 MW power, respectively, and the GTC exports 0.47 MW power to the AC grid in order to maintain the power balance.

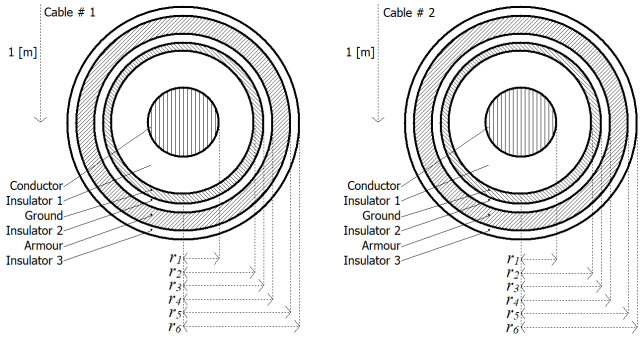

FIGURE 20. Underground cable configuration.

At $t = 1$ s, the total power demand is reduced to 0.69 MW, which leads to voltage rise in the entire DC microgrid, as shown in Fig. 18 (a). The GTC and the BESSs start to absorb larger amounts of power from the DC microgrid to maintain the power balance and limit the voltage rise. At $t = 1.5$ s, the total power demand is further reduced to 0.05 MW (almost no load), which causes the DER voltages to rise again. The GTC reaches its power limit by exporting 1 MW to the AC grid. Thus, the power balance is achieved by increasing the powers drawn by the BESSs and decreasing the power generated by the WT.

As shown in Fig. 18, the DBS control strategy effectively regulates the DC bus voltages and provides acceptable transient response under the maximum power surplus in the grid-connected microgrid. The main shortcoming of the DBS control strategy in this case study is the fact that it causes unnecessary curtailment of the renewable power generation (Fig. 18 (b)) and reduced energy storage by the BESSs (Fig. 18 (c)) that are expected to remain in the full-power charging mode in the grid-connected DC microgrid. The DC microgrid power balance could be restored by increasing the charging currents of the BESSs, without curtailing the WT output power.

As shown in Fig. 19, with the proposed MADC strategy, before $t = 1$ s, the grid-connected DC microgrid is in steady-state, and the DER terminal voltages are between 1 and 1.025 p.u. The WT, PV1 and PV2 operate in MPPT mode and generate 1, 0.5 and 0.5 MW power, respectively, while the total power demand is 1.31 MW. Both BESSs draw their maximum power, i.e. 0.4 MW, and the GTC imports 0.13 MW power from the AC grid.

At $t = 1$ s, the total power demand is reduced to 0.69 MW, which leads to voltage rise in the entire DC microgrid, as shown in Fig. 19 (a). The GTC exports 0.48 MW power to the AC grid to maintain the power balance and limit the voltage rise. Therefore, the DER terminal voltages are regulated at values between 1 p.u. and 1.043 p.u. At $t = 1.5$ s, the total power demand is further reduced to 0.05 MW (almost no load), which causes the DER voltages to rise again. The GTC maintains the power balance by exporting 1.1 MW power to the AC grid. Therefore, the DER terminal voltages are regulated at values between 1 p.u. and 1.06 p.u.

As shown in Fig. 19, the proposed MADC strategy effectively regulates the DC bus voltages without unnecessarily curtailing the renewable power generation. Moreover, all RESs and BESSs operate in the intended modes, i.e. MPPT and charging, respectively, while the GTC regulates the bus voltages of the grid-connected DC microgrid.

V. CONCLUSION

In an islanded DC microgrid that operates based on the conventional MADC strategy, the DERs are responsible for bus voltage regulation. In a realistic DC microgrid, the DERs may fail to perform the necessary mode switching actions due to the unequal bus voltages. The study results presented in this paper indicate that the aforementioned issue may adversely affect the power sharing between the DERs and cause poor voltage regulation in the microgrid. An improved MADC strategy using an adaptive mode switching delay is proposed for reliable and coordinated mode switching by the DERs in the DC microgrid. The results of comprehensive studies conducted on a detailed and realistic study system indicate that:

- the proposed improved MADC strategy effectively regulates the DC bus voltages under various operating conditions, by properly switching the operation modes of the DERs;
- the proposed MADC strategy improves power sharing among the DERs and significantly reduces the circulating currents between the BESSs;
- the adaptive mode switching delay enables reliable and coordinated operation of the DERs controlled based on the MADC strategy, regardless of how fast the bus voltages change in response to disturbances.

VI. FUTURE WORK

The expected future work that can complement this research includes hardware implementation of the proposed improved MADC strategy and testing it in a real DC microgrid platform. The proposed improved MADC strategy can be also utilized in hybrid microgrids. Its effectiveness in coordinated control of the DERs and loads in a hybrid microgrid will be investigated in future studies.

APPENDIX

The parameters of the DC microgrid study system of Fig. 9 [44], and the coefficients of the PI controllers of the DERs, are provided in this appendix. Table 2 provides the ratings and parameters of the converters utilized in the DC microgrid. Four different types, i.e., sizes, of the 1 kV single-core XLPE cable [50] are used in the study system, depending on the ampacity of each feeder section to ensure the power loss and voltage drop of each line segment is below the permitted limits. The positive and negative polarity underground cables are assumed to be buried 1 m deep, with a horizontal separation of 0.5 m. Table 3 shows the per-unit-length parameters of each cable type. Fig. 20 shows the general configuration of the underground cable, which

TABLE 2. Parameters of the DC microgrid.

GTC	$S_{Transformer}$ = 2 MVA	Trans. Ratio: 0.75kV/4.8 kV
	S_{GTC} = 2 MVA	C_{dc} = 40 mF
	V_{rated} = 750 V	f_{sw} = 2.7 kHz
WT	P_{WT} = 1 MW	V_{rated} = 690 V
	S_{PMSG} = 1.1 MVA	S_{MSC} = 1.1 MVA
	ω_b = 377 rad/s	f_{rated} = 60 Hz
	R_s = 0.017 pu	X_l = 0.064 pu
	X_d = 0.55 pu	X_q = 1.1 pu
	R_{kd} = 0.055 pu	R_{kq} = 0.183 pu
	X_{kd} = 0.62 pu	X_{kq} = 1.175 pu
	Ψ_f = 1 pu	C_{dc} = 20 mF
PV	P_{PV} = 2*0.5 MW = 1 MW	Irradiation = 0-1000 w/m^2
	V_{OC} = 973.7 V	I_{SC} = 714 A
	C_{dc} = 10 mF	f_{sw} = 2.7 kHz
BESS	P_{BESS} = 2*0.4 MW = 0.8 MW	V_{rated} = 0.7 kV
	Capacity = 0.57 kAh	C_{dc} = 10 mF

TABLE 3. Underground cable parameters per unit length.

Type	1	2	3	4
Size	1000 kcmil	250 kcmil	1 AWG	6 AWG
***R* (mΩ/m)**	0.075	0.232	0.599	1.701
***L* (μH/m)**	0.118	0.181	0.262	0.366
***C* (nF/m)**	0.402	0.216	0.152	0.120

TABLE 4. Underground cable dimensions.

Type	**Size**	**Dimensions (mm)**					
		r_1	r_2	r_3	r_4	r_5	r_6
1	1000 kcmil	12.7	14.99	18.1	19.62	24.08	25.54
2	250 kcmil	6.35	8.64	10.635	12.155	15.645	16.99
3	1 AWG	3.674	5.704	7.21	8.35	11.405	12.65
4	6 AWG	2.057	3.577	4.99	5.75	8.8	10.045

TABLE 5. Parameters of the PI controllers [p.u.].

DER	**PI-Controlled Variable**	K_P	T_I	**Output Limits**
WT	Stator Currents I_{sq} and I_{sd}	0.5	0.01	-1.3 to 1.3
	Active Power P_{PMSG}	0.2	0.01	0 to 1
	Stator Voltage V_s	2	0.02	-1 to 1
	DC-terminal Voltage V_{DC}	5	0.003	0 to 1
PV	PV Voltage V_{PV}	2	0.005	0 to 1
	DC-terminal Voltage V_{DC}	2	0.005	0 to 1
BESS	Battery Current I_{BESS}	2	0.01	0 to 1
	Battery Voltage V_{BESS}	20	0.001	0 to 1
	DC-Terminal Current I_{dc}	0.1	0.08	-1 to 1
	DC-Terminal Voltage V_{dc}	20	0.002	-1 to 1

applies to all four types. Table 4 shows the dimensions of each cable type. Table 5 provides the coefficients and output limits of the PI controllers shown in Figs. 6-8.

REFERENCES

[1] J. J. Justo, F. Mwasilu, J. Lee, and J.-W. Jung, "AC-microgrids versus DC-microgrids with distributed energy resources: A review," *Renew. Sustain. Energy Rev.*, vol. 24, pp. 387–405, Aug. 2013.
[2] E. Planas, J. Andreu, J. I. Gárate, I. M. De Alegría, and E. Ibarra, "AC and DC technology in microgrids: A review," *Renew. Sustain. Energy Rev.*, vol. 43, pp. 726–749, Mar. 2015.
[3] S. Parhizi, H. Lotfi, A. Khodaei, and S. Bahramirad, "State of the art in research on microgrids: A review," *IEEE Access*, vol. 3, pp. 890–925, 2015.
[4] D. Kumar, F. Zare, and A. Ghosh, "DC microgrid technology: System architectures, AC grid interfaces, grounding schemes, power quality, communication networks, applications, and standardizations aspects," *IEEE Access*, vol. 5, pp. 12230–12256, 2017.
[5] T. Dragičević, X. Lu, J. C. Vasquez, J. M. Guerrero, "DC microgrids—Part II: A review of power architectures, applications, and standardization issues," *IEEE Trans. Power Electron.*, vol. 31, no. 5, pp. 3528–3549, May 2016.
[6] S. K. Sahoo, A. K. Sinha, and N. K. Kishore, "Control techniques in AC, DC, and hybrid AC–DC microgrid: A review," *IEEE J. Emerg. Sel. Topics Power Electron.*, vol. 6, no. 2, pp. 738–759, Jun. 2018.
[7] T. Dragičević, X. Lu, J. C. Vasquez, J. M. Guerrero, "DC microgrids—Part I: A review of control strategies and stabilization techniques," *IEEE Trans. Power Electron.*, vol. 31, no. 7, pp. 4876–4891, Jul. 2016.
[8] J. P. Torreglosa, P. García-Triviño, L. M. Fernández-Ramirez, and F. Jurado, "Control strategies for DC networks: A systematic literature review," *Renew. Sustain. Energy Rev.*, vol. 58, pp. 319–330, May 2016.
[9] L. Meng, Q. Shafiee, G. F. Trecate, H. Karimi, D. Fulwani, X. Lu, and J. M. Guerrero, "Review on control of DC microgrids and multiple microgrid clusters," *IEEE J. Emerg. Sel. Topics Power Electron.*, vol. 5, no. 3, pp. 928–948, Sep. 2017.
[10] A. G. Tsikalakis and N. D. Hatziargyriou, "Centralized control for optimizing microgrids operation," *IEEE Trans. Energy Convers.*, vol. 23, no. 1, pp. 241–248, Mar. 2008.
[11] K. T. Tan, X. Y. Peng, P. L. So, Y. C. Chu, and M. Z. Q. Chen, "Centralized control for parallel operation of distributed generation inverters in microgrids," *IEEE Trans. Smart Grid*, vol. SG-3, no. 4, pp. 1977–1987, Dec. 2012.
[12] J. Rajagopalan, K. Xing, Y. Guo, F. C. Lee, and B. Manners, "Modeling and dynamic analysis of paralleled dc/dc converters with master-slave current sharing control," in *Proc. IEEE Appl. Power Electron. Conf. (APEC)*, San Jose, CA, USA, vol. 2, Mar. 1996, pp. 678–684.
[13] T.-F. Wu, Y.-K. Chen, and Y.-H. Huang, "3C strategy for inverters in parallel operation achieving an equal current distribution," *IEEE Trans. Ind. Electron.*, vol. 47, no. 2, pp. 273–281, Apr. 2000.
[14] D.-H. Dam and H.-H. Lee, "A power distributed control method for proportional load power sharing and bus voltage restoration in a DC microgrid," *IEEE Trans. Ind. Appl.*, vol. 54, no. 4, pp. 3616–3625, Jul./Aug. 2018.
[15] F. Guo, Q. Xu, C. Wen, L. Wang, and P. Wang, "Distributed secondary control for power allocation and voltage restoration in islanded DC microgrids," *IEEE Trans. Sustain. Energy*, vol. 9, no. 4, pp. 1857–1869, Oct. 2018.
[16] R. Han, L. Meng, J. M. Guerrero, and J. C. Vasquez, "Distributed nonlinear control with event-triggered communication to achieve current-sharing and voltage regulation in DC microgrids," *IEEE Trans. Power Electron.*, vol. 33, no. 7, pp. 6416–6433, Jul. 2018. doi: 10.1109/TPEL.2017.2749518.
[17] L. Che and M. Shahidehpour, "DC microgrids: Economic operation and enhancement of resilience by hierarchical control," *IEEE Trans. Smart Grid*, vol. 5, no. 5, pp. 2517–2526, Sep. 2014.
[18] C. Jin, P. Wang, J. Xiao, Y. Tang, and F. H. Choo, "Implementation of hierarchical control in DC microgrids," *IEEE Trans. Ind. Electron.*, vol. 61, no. 8, pp. 4032–4042, Aug. 2014.
[19] Q. Shafiee, T. Dragičević, J. C. Vasquez, and J. M. Guerrero, "Hierarchical control for multiple DC-microgrids clusters," *IEEE Trans. Energy Convers.*, vol. 29, no. 4, pp. 922–933, Dec. 2014.
[20] C. Wang, J. Duan, B. Fan, Q. Yang, and W. Liu, "Decentralized high-performance control of DC microgrids," *IEEE Trans. Smart Grid*, vol. 10, no. 3, pp. 3355–3363, May 2019.
[21] P. Sanjeev, N. P. Padhy, and P. Agarwal, "Autonomous power control and management between standalone DC microgrids," *IEEE Trans. Ind. Inform.*, vol. 14, no. 7, pp. 2941–2950, Jul. 2018.

[22] S. Peyghami, H. Mokhtari, P. Davari, P. C. Loh, and F. Blaabjerg, "On secondary control approaches for voltage regulation in DC microgrids," *IEEE Trans. Ind. Appl.*, vol. 53, no. 5, pp. 4855–4862, Sep./Oct. 2017.

[23] P. Prabhakaran, Y. Goyal, and V. Agarwal, "Novel nonlinear droop control techniques to overcome the load sharing and voltage regulation issues in DC microgrid," *IEEE Trans. Power Electron.*, vol. 33, no. 5, pp. 4477–4487, May 2018.

[24] X. Lu, K. Sun, J. M. Guerrero, J. C. Vasquez, and L. Huang, "State-of-charge balance using adaptive droop control for distributed energy storage systems in DC microgrid applications," *IEEE Trans. Ind. Electron.*, vol. 61, no. 6, pp. 2804–2815, Jun. 2014.

[25] X. Lu, K. Sun, J. M. Guerrero, J. C. Vasquez, and L. Huang, "Double-quadrant state-of-charge-based droop control method for distributed energy storage systems in autonomous DC microgrids," *IEEE Trans. Smart Grid*, vol. 6, no. 1, pp. 147–157, Jan. 2015.

[26] S. Augustine, M. K. Mishra, and N. Lakshminarasamma, "Adaptive droop control strategy for load sharing and circulating current minimization in low-voltage standalone DC microgrid," *IEEE Trans. Sustain. Energy*, vol. 6, no. 1, pp. 132–141, Jan. 2015.

[27] J. Schonbergerschonberger, R. Duke, S. D. Round, "DC-bus signaling: A distributed control strategy for a hybrid renewable nanogrid," *IEEE Trans. Ind. Electron.*, vol. 53, no. 5, pp. 1453–1460, Oct. 2006.

[28] K. Sun, L. Zhang, Y. Xing, and J. M. Guerrero, "A distributed control strategy based on DC bus signaling for modular photovoltaic generation systems with battery energy storage," *IEEE Trans. Power Electron.*, vol. 26, no. 10, pp. 3032–3045, Oct. 2011.

[29] N. Eghtedarpour and E. Farjah, "Control strategy for distributed integration of photovoltaic and energy storage systems in DC micro-grids," *Renew. Energy*, vol. 45, pp. 96–110, Sep. 2012.

[30] D. Chen, L. Xu, and L. Yao, "DC voltage variation based autonomous control of DC microgrids," *IEEE Trans. Power Del.*, vol. 28, no. 2, pp. 637–648, Apr. 2013.

[31] Y. Gu, X. Xiang, W. Li, and X. He, "Mode-adaptive decentralized control for renewable DC microgrid with enhanced reliability and flexibility," *IEEE Trans. Power Electron.*, vol. 29, no. 9, pp. 5072–5080, Sep. 2014.

[32] D. Wu, F. Tang, T. Dragičević, J. M. Guerrero, and J. C. Vasquez, "Coordinated control based on bus-signaling and virtual inertia for islanded DC microgrids," *IEEE Trans. Smart Grid*, vol. 6, no. 6, pp. 2627–2638, Nov. 2015.

[33] Y. Gu, W. Li, and X. He, "Frequency-coordinating virtual impedance for autonomous power management of dc microgrid," *IEEE Trans. Power Electron.*, vol. 30, no. 4, pp. 2328–2337, Apr. 2015.

[34] L. Gao, Y. Liu, H. Ren, and J. Guerrero, "A DC microgrid coordinated control strategy based on integrator current-sharing," *Energies*, vol. 10, no. 8, p. 1116, Aug. 2017.

[35] J. Meng, Y. Wang, C. Wang, and H. Wang, "Design and implementation of hardware-in-the-loop simulation system for testing control and operation of DC microgrid with multiple distributed generation units," *IET Gener., Transmiss. Distrib.*, vol. 11, no. 12, pp. 3065–3072, Aug. 2017.

[36] Y. Wang, M. Yu, and Y. Li, "Self-adaptive inertia control of DC microgrid based on fast predictive converter regulation," *IET Renew. Power Gener.*, vol. 11, no. 8, pp. 1295–1303, Jun. 2017.

[37] Y. Xia, M. Yu, P. Yang, Y. Peng, and W. Wei, "Generation-storage coordination for islanded DC microgrids dominated by PV generators," *IEEE Trans. Energy Convers.*, vol. 34, no. 1, pp. 130–138, Mar. 2019.

[38] N. L. Diaz, T. Dragičević, J. C. Vasquez, J. M. Guerrerom, "Intelligent distributed generation and storage units for DC microgrids—A new concept on cooperative control without communications beyond droop control," *IEEE Trans. Smart Grid*, vol. 5, no. 5, pp. 2476–2485, Sep. 2014.

[39] Q. Yang, L. Jiang, H. Zhao, and H. Zeng, "Autonomous voltage regulation and current sharing in islanded multi-inverter DC microgrid," *IEEE Trans. Smart Grid*, vol. 9, no. 6, pp. 6429–6437, Nov. 2018.

[40] D. Chen and L. Xu, "Autonomous DC voltage control of a DC microgrid with multiple slack terminals," *IEEE Trans. Power Syst.*, vol. 27, no. 4, pp. 1897–1905, Nov. 2012.

[41] L. Xu and D. Chen, "Control and operation of a DC microgrid with variable generation and energy storage," *IEEE Trans. Power Del.*, vol. 26, no. 4, pp. 2513–2522, Oct. 2011.

[42] A. Khorsandi, M. Ashourloo, and H. Mokhtari, "A decentralized control method for a low voltage DC microgrid," *IEEE Trans. Energy Convers.*, vol. 29, no. 4, pp. 793–801, Dec. 2014.

[43] T. Dragičević, J. M. Guerrero, J. C. Vasquez, and D. Škrlec, "Supervisory control of an adaptive-droop regulated dc microgrid with battery management capability," *IEEE Trans. Power Electron.*, vol. 29, no. 2, pp. 695–706, Feb. 2014.

[44] J. Mohammadi and F. B. Ajaei, "Versatile decentralized control of the DC microgrid," *IET Smart Grid*, vol. 2, no. 1, pp. 77–88, Mar. 2019.

[45] K. Li, "PID tuning for optimal closed-loop performance with specified gain and phase margins," *IEEE Trans. Control Syst. Technol.*, vol. 21, no. 3, pp. 1024–1030, May 2013.

[46] B. Yang, X. Zhang, T. Yu, H. Shu, and Z. Fang, "Grouped grey wolf optimizer for maximum power point tracking of doubly-fed induction generator based wind turbine," *Energy Convers. Manage.*, vol. 133, pp. 427–443, Feb. 2017.

[47] B. Yang, T. Yu, H. Shu, X. Zhang, K. Qu, and L. Jiang, "Democratic joint operations algorithm for optimal power extraction of PMSG based wind energy conversion system," *Energy Convers. Manage.*, vol. 159, pp. 312–326, Mar. 2018.

[48] *IEEE 37 Node Test Feeder, IEEE Distribution Test Feeder Working Group Report*. Accessed: 1992. [Online]. Available: http://sites.ieee.org/pes-testfeeders/resources/

[49] E. Rodriguez-Diaz, F. Chen, J. C. Vasquez, J. M. Guerrero, R. Burgos, and D. Boroyevich, "Voltage-level selection of future two-level LVdc distribution grids: A compromise between grid compatibiliy, safety, and efficiency," *IEEE Electrific. Mag.*, vol. 4, no. 2, pp. 20–28, Jun. 2016.

[50] *General Cable, 600V-28kV TECK90 XLPE/PVC/AIA/PVC Armored Control and Power Cables*. Accessed: Sep. 2016. [Online]. Available: http://www.generalcable.com

JAFAR MOHAMMADI (S'17) received the B.Sc. degree in electrical engineering from the University of Mazandaran, Iran, in 2009, and the M.Sc. degree in electrical engineering from the University of Tehran, Tehran, Iran, in 2012. He is currently pursuing the Ph.D. degree with the Department of Electrical and Computer Engineering, Western University, Canada.

His research interest includes the control and protection of power systems, especially microgrids and renewable energy systems.

FIROUZ BADRKHANI AJAEI (S'12–M'15) received the B.Sc. degree from Tehran Polytechnic University, Iran, in 2006, the M.Sc. degree from the University of Tehran, Iran, in 2009, and the Ph.D. degree from the University of Toronto, Canada, in 2015, all in electrical engineering.

He is currently an Assistant Professor with the Department of Electrical and Computer Engineering, Western University, Canada. His research interests include the protection and control of power systems with focus on renewable energy systems, microgrids, and dc–ac grids.